Supplemental Figure 1. Synthetic HBD does not bind hepcidin-25 specifically. Surface plasmon resonance analysis of HBD interaction with hepcidin: **A**. WT HBD or C326S HBD mutant was coated on the sensor surface, and bioactive hepcidin-25 or inactive hepcidin-20 were injected as analytes. There was no difference in hepcidin binding to HBD and mutated HBD-C326S. **B**. Hepcidin-25 but not hepcidin-20 aggregated on the sensor surface coated with hepcidin-25 itself, streptavidin (SA) or hepcidin biotinylated at K18 residue. **C**. The reverse configuration, with hepcidin-25 or -20 coated on the chip and HBD used as analyte, generated a negative binding signal, i.e. HBD bound to hepcidin less than it did to the uncoated reference sensor surface.

Although not shown in the figure, additional surface plasmon resonance experiments support the argument that HBD is not a hepcidin-binding domain: 1) Hepcidin bound similarly to unalkylated and alkylated HBD, whereas alkylation of cells expressing ferroportin-GFP prevented hepcidin binding. 2) Bioactive mouse hepcidin did not bind to HBD. 3) Non-aggregating but bioactive hepcidin derivatives (M21Y-hepcidin, F4Nleu-hepcidin, minihepcidin hep9) did not bind to HBD. 4) Aggregating mutant (hepcidin-protegrin chimera) which was inactive in cellular assays did bind HBD. Furthermore, using competitive ELISA format, we found no competition between unlabeled hepcidin and any of the three biotinylated hepcidins (N-terminal, K18 and K24-biotinylated) for HBD-coated plates. We did not detect any competition between unlabeled and ^{125}I-hepcidin for HBD-coated beads.

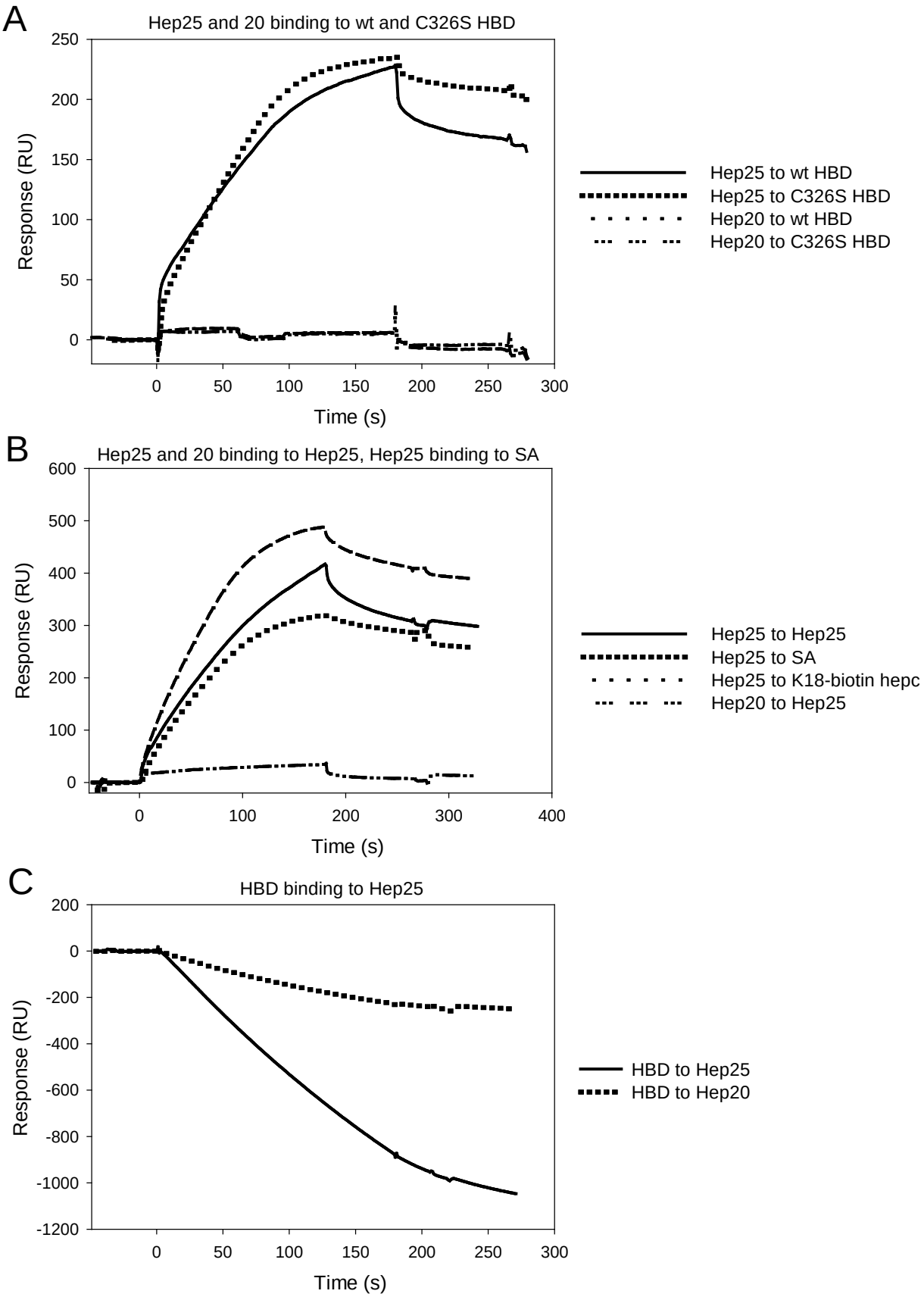
A
Hep25 and 20 binding to wt and C326S HBD
Response (RU)
Time (s)
Hep25 to wt HBD
Hep25 to C326S HBD
Hep20 to wt HBD
Hep20 to C326S HBD
B
Hep25 and 20 binding to Hep25, Hep25 binding to SA
Response (RU)
Time (s)
Hep25 to Hep25
Hep25 to SA
Hep25 to K18-biotin hepc
Hep20 to Hep25
C
HBD binding to Hep25
Response (RU)
Time (s)
HBD to Hep25
HBD to Hep20

Supplemental Figure 2. Fluorescent microscopy of Fpn-GFP mutants from Figure 1C/D. Most mutants were expressed on the plasma membrane, but some (D325N, I327A, A332D) had prominent intracellular localization.

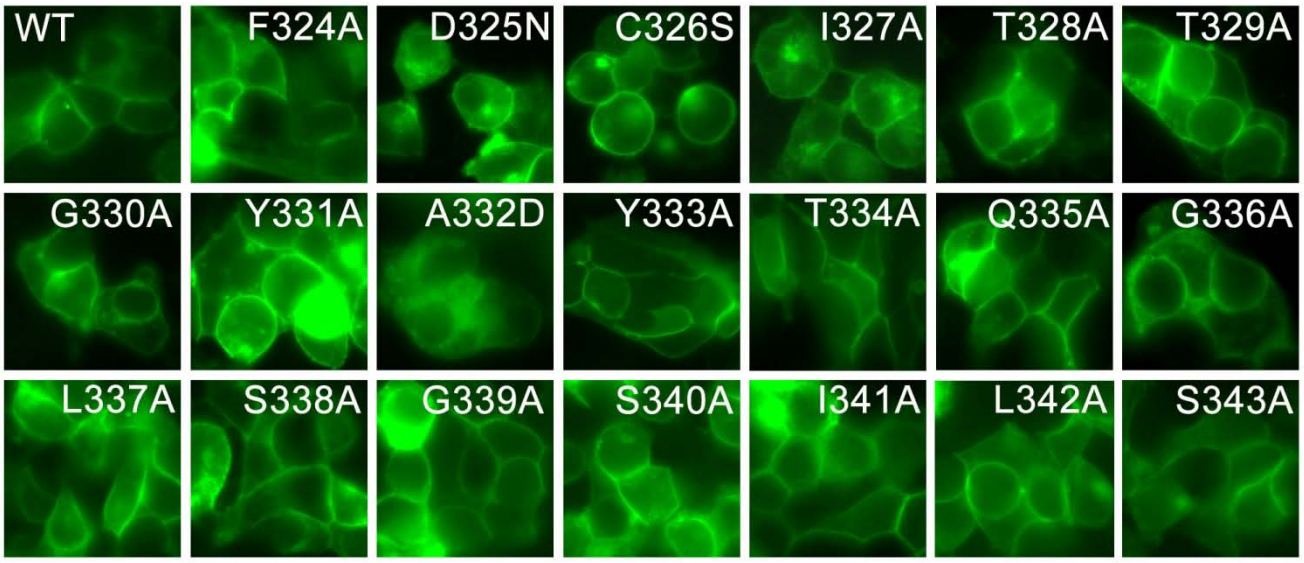

Supplemental Figure 3. Circular dichroism spectroscopy of hepcidin disulfide mutants. Circular dichroism spectroscopy was used to assess changes in the secondary structure of hepcidin disulfide mutants. **A.** The solid line represents the spectrum of the native hepcidin, and dashed lines the spectra of hepcidin mutants. **B.** Quantitative analysis of the spectra. Estimates of the secondary structure were made with SELCON algorithm using the spectral basis set SP43, and results expressed as percentage of conformations.

A.

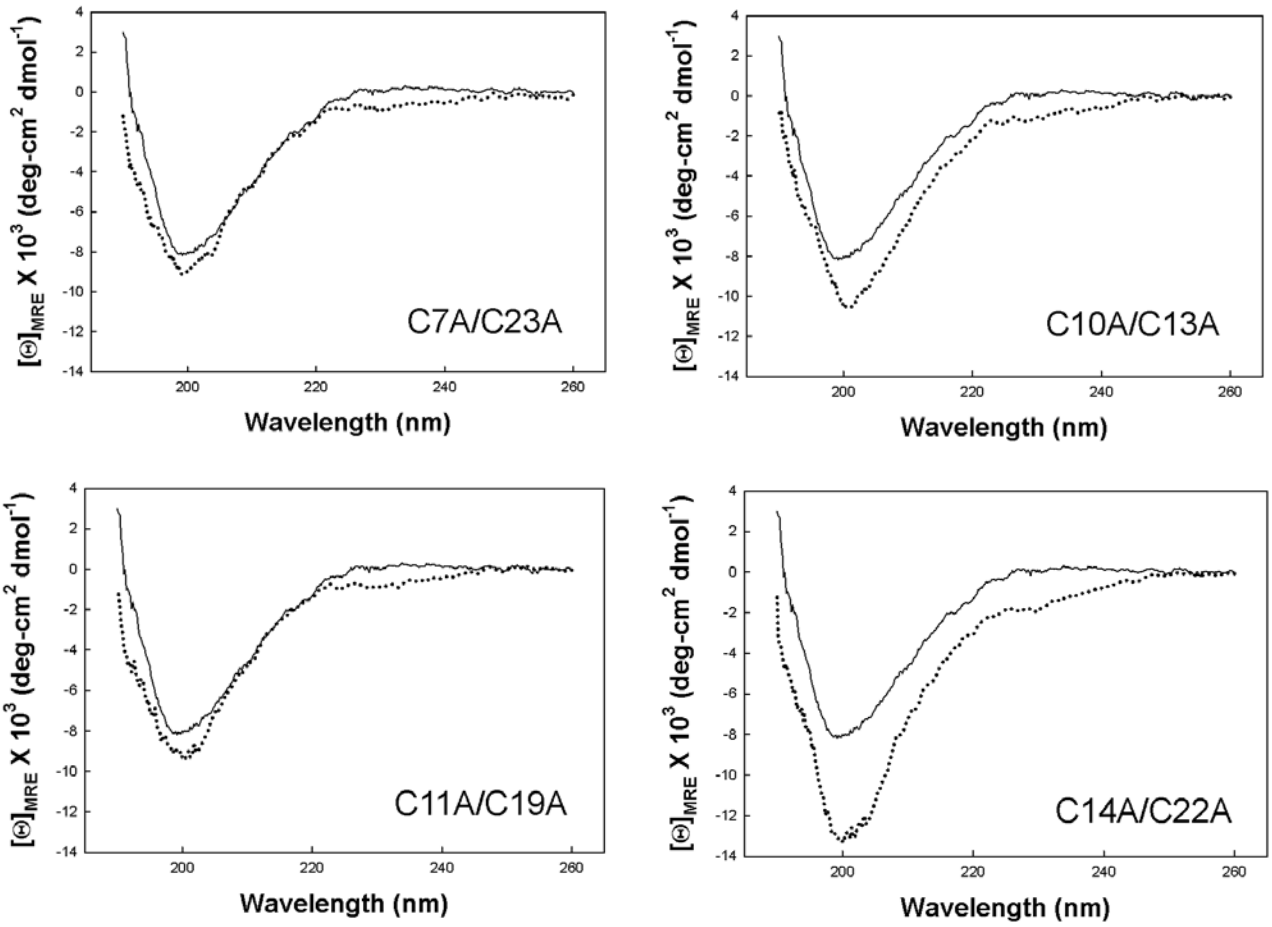

B.

Sample	% beta sheet	% disordered beta sheet	% disordered	% turn
Hepcidin25	29	14	36	21
C7A/C23A	27	14	40	19
C10A/C13A	27	14	40	19
C11A/C19A	27	14	40	19
C14A/C22A	26	14	41	19

Supplemental Figure 4. A RosettaDock model of the hepcidin-ferroportin interface. The model is identical to the one in Figure 3, but is viewed parallel to the interface of the two molecules. Hepcidin on the top is shown in pink with yellow disulfide connectivities. Ferroportin extracellular loop on the bottom is shown in cyan, transmembrane helices in grey, and the sulfur of C326 in yellow. The strongly interacting side chain pairs are displayed in thicker lines.

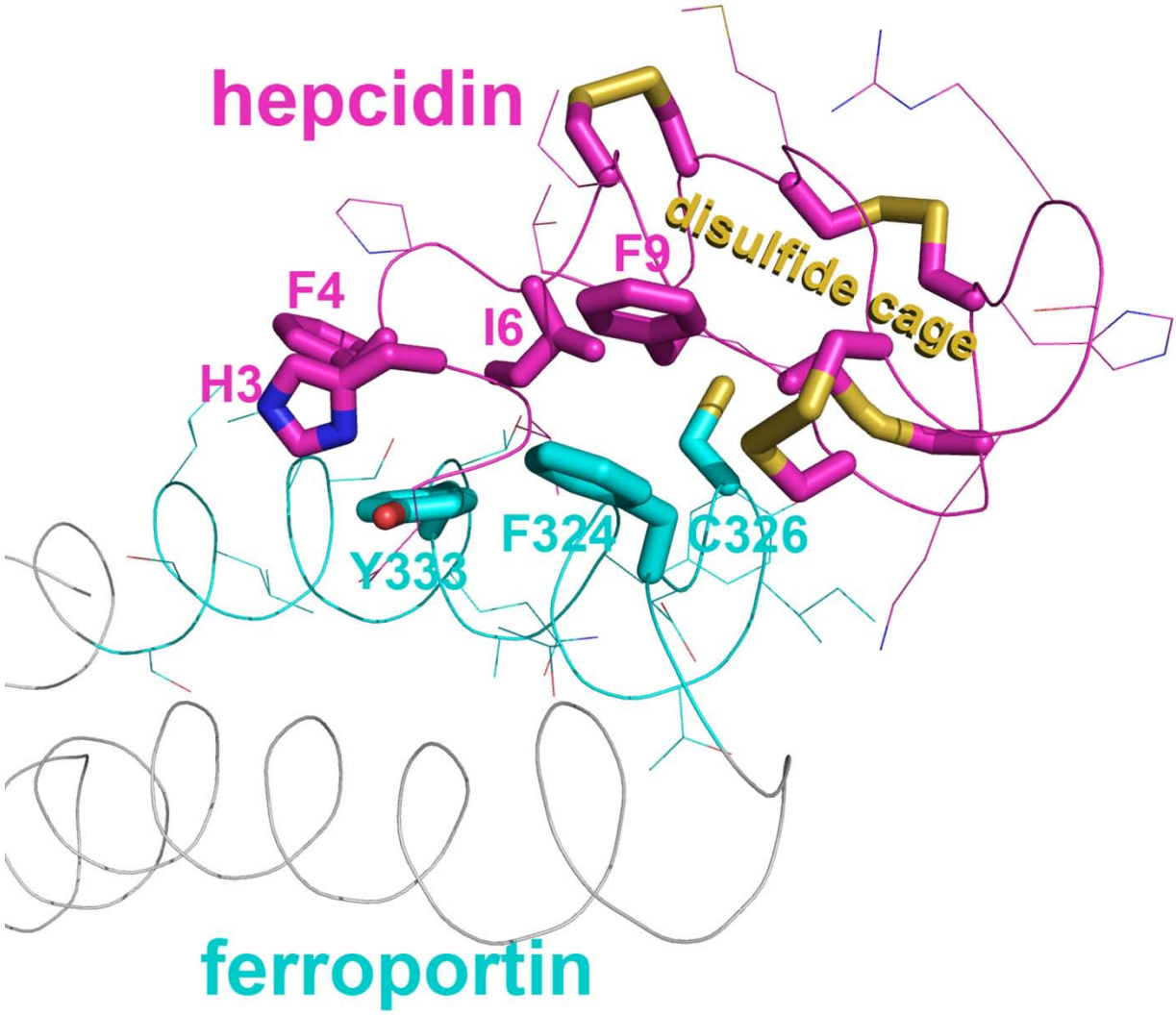

Supplemental Figure 5. Modeled structure of the minihepcidin composed of 9 N-terminal residues of human hepcidin (DTHFPICIF). The structure was generated using PyMOL software.

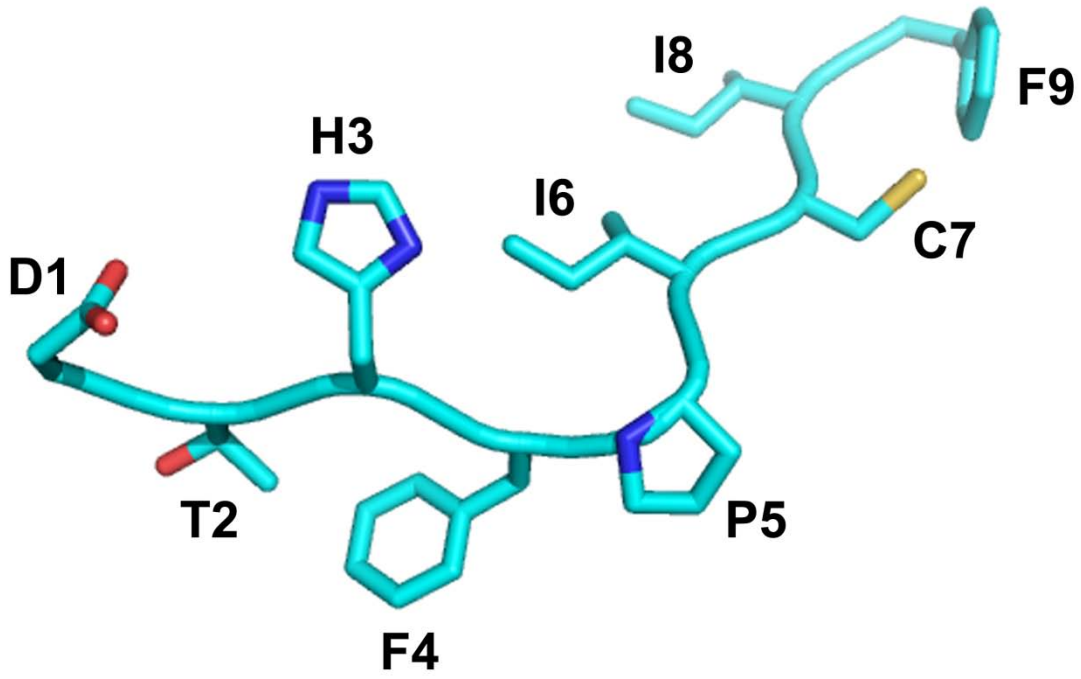

Supplemental Figure 6. Minihepcidin lacking cysteine is not active *in vivo*. Palmitoylated retroinverted hep9 (palm-ri-hep9) which contains a single cysteine was synthesized with the cysteine to serine substitution (palm-ri-hep9-Ser). Both peptides were injected intraperitoneally (20 nmoles per mouse, n=4 animals per treatment), mice were euthanized after 4 h, and non-heme iron levels determined in serum.

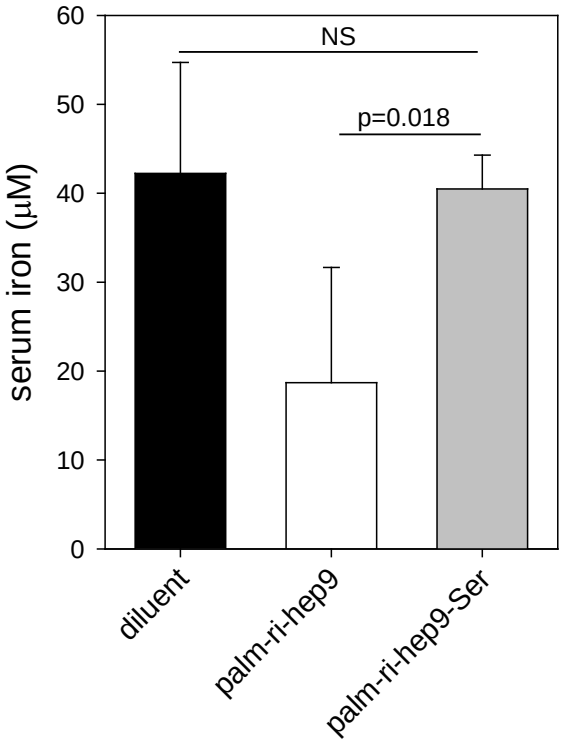

Supplemental Figure 7. Administration of minihepcidins in mice did not increase the expression of endogenous hepatic hepcidin mRNA. Hepcidin mRNA was measured by qPCR and normalized to the expression of actin mRNA. Graphs show mean and standard deviation of hepcidin ddCt. **A.** Hepcidin expression in mice from Figure 6B (intraperitoneal injection of minihepcidins). **B.** Hepcidin expression in mice from Figure 6C (oral administration by gavage). Only the gavage of full-length hepcidin-25 but not minihepcidins induced endogenous hepcidin mRNA (p=0.02).

A.

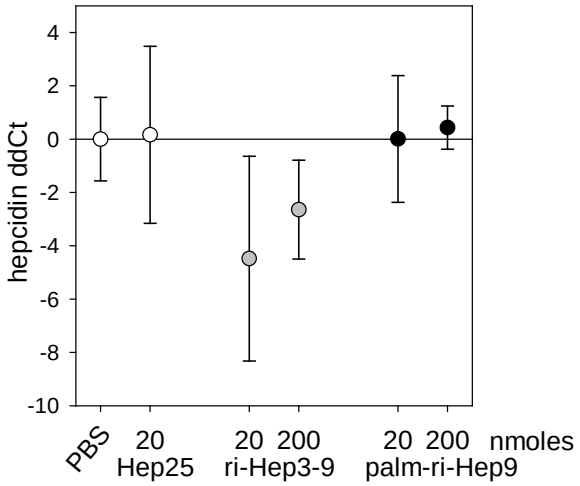

B.

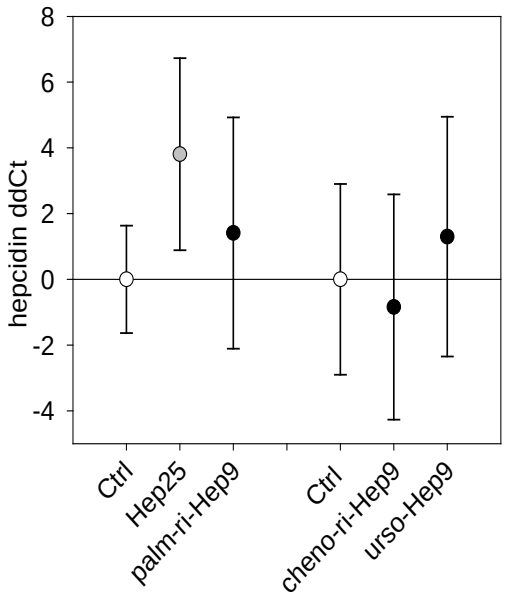

Supplemental Table 1. RosettaDock-derived pair energies across hepcidin-ferroportin interface showing strong association of ligand-receptor residues in the hypothetical molecular complex.

Fpn aa		Hep aa		total energy
323	GLY	18	LYS	0.15
323	GLY	19	CYS	0.01
324	PHE	1	ASP	-0.19
324	PHE	2	THR	-0.25
324	PHE	9	PHE	-1.93
324	PHE	11	CYS	0.71
324	PHE	19	CYS	-0.06
325	ASP	2	THR	-0.48
325	ASP	9	PHE	-0.05
325	ASP	10	CYS	-0.16
325	ASP	11	CYS	-1.96
325	ASP	12	GLY	0.01
325	ASP	13	CYS	0.01
326	CYS	2	THR	-0.23
326	CYS	6	ILE	0.10
326	CYS	9	PHE	0.04
326	CYS	10	CYS	-0.52
326	CYS	11	CYS	-0.05
326	CYS	13	CYS	-0.14
326	CYS	22	CYS	0.00
326	CYS	24	LYS	-0.15
327	ILE	10	CYS	-0.02
327	ILE	12	GLY	-0.01
327	ILE	13	CYS	-0.15
329	THR	1	ASP	0.01
329	THR	2	THR	-0.19
330	GLY	2	THR	-0.04
330	GLY	6	ILE	-0.32
331	TYR	24	LYS	-0.78
333	TYR	1	ASP	-0.28
333	TYR	2	THR	-0.28
333	TYR	3	HIS	-0.44
333	TYR	4	PHE	-1.60
333	TYR	6	ILE	-0.96
333	TYR	25	THR	0.00
334	THR	4	PHE	-0.03
334	THR	6	ILE	0.01
334	THR	24	LYS	0.02
337	LEU	4	PHE	-0.61

Supplemental Table 2. Design and bioassay of modified minihepcidins. Peptide sequences and IC50 values are displayed. IC50 was calculated from peptide dose response studies in which the activity was quantitated by measuring Fpn-GFP degradation by flow cytometry. Some peptides were synthesized as carboxyamides. D amino acids are represented by blue font. Unnatural amino acids are indicated in red and their structure is displayed in the Supplemental Table 3. ChenoD = chenodeoxycholic acid, or UrsoD = ursodeoxycholic acid, BetaP = Beta propeller, CD = collagen domain.

	Peptide Name	**Sequence**	**IC50 (μM)**
Minihepcidins	Hep1-9	DTHFPICIF	0.076
	Hep1-8	DTHFPICI	2.5
	Hep1-7	DTHFPIC	10
	Hep4-7	FPIC	7.5
	Hep3-7	HFPIC	10
	Hep3-8	HFPICI	1
	Hep3-9	HFPICIF	0.55
Cysteine Modifications of Hep1-9	Hep1-9 dC	DTHFPIdCIFamide	inactive (>10)
	Hep1-9 homoC	DTHFPIhomoCIFamide	0.3
	Hep1-9 Pen	DTHFPIPenIFamide	Inactive (>10)
	Hep1-9 dPen	DTHFPIdPenIFamide	Inactive (>10)
	Hep1-9 Dap(AcBr)	DTHFPIDap(AcBr)IFamide	Inactive (>10)
Cyclic peptides	Cyc-1	CDTHFPICIFamide	0.3
	Cyc-2	DTHFPICIF-$CONH_2$-CH_2-CH_2-S	Inactive (>10)
	Cyc-3	CHFPICIFamide	Inactive (>10)
	Cyc-4	HFPICIF-$CONH_2$-CH_2-CH_2-S	Inactive (>10)
Unnatural aa's	Un Pr10	DTleHPhgOicChgCChgFamide	Inactive (>10)
	Un Pr11	DTleHPOicChgCChgFamide	Inactive (>10)
Retro-Inverso Modifications	ri-Hep1-9	FICIPFHTD	0.8
	ri-Hep3-9	FICIPFH	0.2
	ChenoD-ri-Hep1-9	ChenoD(PEG11)**FICIPFHTD**amide	0.10
	UrsoD-ri-Hep1-9	UrsoD(PEG11)**FICIPFHTD**amide	1
	ri-Hep1-9 BetaP	**FICIPFHTD**(PEG11)-GYIPEAPRDGQAYVRKDGEWVLLSTFLamide	Inactive (>10)
	ri-Hep1-9 CD	**FICIPFHTD**(PEG11)-(GPHyp)10-amide	Inactive (>10)
	Palm-ri-Hep1-9	Palmitoyl-(PEG11)-**FICIPFHTD**amide	0.01
	Palm-ri-Hep1-9-	Palmitoyl-(PEG11)-**FISIPFHTD**amide	Inactive
	2Palmitoyl ri-	2(Palmitoyl)-Dap(PEG11)-**FICIPFHTD**amide	2

Supplemental Table 3. Uncommon or Unnatural Amino Acids

Chg 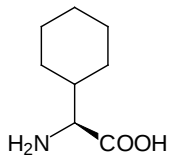 L-α-cyclohexylglycine	**Tle** 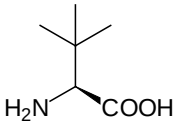 L-tert-leucine	**Phg** 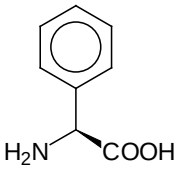 L-phenylglycine	**Pen** 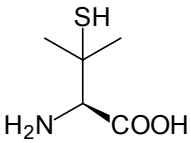 L-Penicillamine	**(D)Pen** 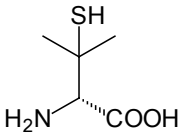 D-Penicillamine
Oic 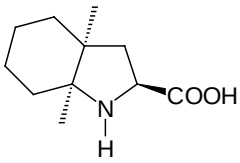 octahydroindole-2-carboxylic acid	**Dap(AcBr)** 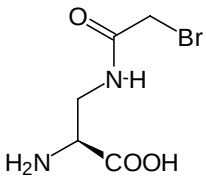 N^{γ}-(bromoacetyl)-L-2,3-diaminopropionic acid	**Cys(tBut)** 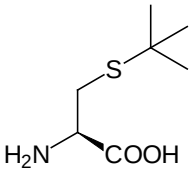 S-t-butyl-L-cysteine	**HomoC** 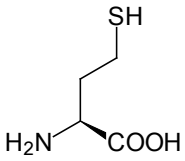 L-homocysteine	**Cys(S-tBut)** 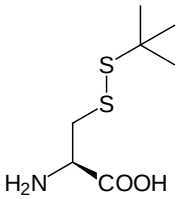 S-t-Butylthio-L-cysteine